eJSE International

Special Issue: Electronic Journal of Structural Engineering 14(1) 2015

Crack Detection using a Texture Analysis-based Technique for Visual Bridge Inspection

G.P. Bu[1], S. Chanda[2], H. Guan[1], J. Jo[2], M. Blumenstein[2] & Y.C. Loo[1]

[1]*School of Engineering, Griffith University, Queensland, Australia*

[2]*School of Information and Communication Technology, Griffith University, Queensland, Australia*

Email: h.guan@griffith.edu.au

ABSTRACT: Bridge inspection is a pathway to bridge condition rating assessment, and is an essential element of any bridge management system (BMS). The success of a BMS is highly dependent on the quality of bridge inspection outcomes and accurate estimation of future bridge condition ratings. However, existing visual bridge inspection methods suffer several limitations due to human subjective judgment. In order to minimise such limitations, a feasibility study has been performed to enhance the current visual inspection method using optical image processing techniques. However, the accuracy of the inspection outcomes still requires further improvement. This paper proposes an automatic bridge inspection approach employing wavelet-based image features along with support vector machines (SVM) for automatic detection of cracks in bridge images. A two-stage approach is followed, in the first stage, a decision is made as whether an image should undergo a pre-processing step (depending on image characteristics); in the second stage, wavelet features are extracted from the image using a sliding window texture analysis-based technique. Consequently, an average accuracy of 92% (effect of training image types on accuracy) is obtained even when undertaking experiments with noisy and complex bridge images.

Keywords: Bridge inspection, condition ratings, bridge management system (BMS), wavelet-based crack detection, texture analysis-based technique, bridge images.

1. INTRODUCTION

Bridges are essential components of any transportation infrastructure, which requires timely decision-making for maintenance, repair and rehabilitation (MR&R) operations. For effective asset management, many bridge authorities have implemented bridge management systems (BMSs) to manage their routine inspection information and to establish MR&R strategies. To ensure such successful outcomes, BMSs must (1) contain reliable, consistent and accurate condition data from routine bridge inspections; and (2) encompass reliable deterioration modelling that overcomes the shortcomings of the lack of historical bridge inspection records. However, without consistent and accurate bridge condition data, reliable BMS outcomes cannot be expected regardless of the superiority of the asset management techniques. Routine bridge inspections are a convenient way of evaluating the overall safety and performance of a bridge and a significant practice to reliably operate BMSs, because the success of a BMS is highly dependent on the quality of bridge inspection records. To evaluate the bridge condition status, inspections are regularly scheduled and performed visually by qualified bridge inspectors with a minimum amount of equipment.

Although current routine inspections are required to be carried out by certified inspectors to provide condition assessment, some major issues have been identified: (i) visual inspections are subjective and not always reliable (Phares et al. 2004; Moore et al. 2001). Routine inspections are operated by qualified bridge inspectors to assess the condition ratings underneath the bridge by measuring its deterioration status. The reliability of the degree of defects is completely dependent on the inspector's knowledge and experience. For this reason, the bridge condition assessment outcomes are occasionally error-prone and have wide variations amongst inspectors. Thus, it is difficult to objectively assess the deterioration status of a bridge through standard visual inspection. This in turn increases the degree of temporal uncertainty in predicting long-term bridge element performance; (ii) the entire manual inspection process is time-consuming and costly (Chase and Edwards 2011; Sanford et al. 1999), especially when the bridge is extremely long or spans a substantial area, which substantially increases the total inspection cost. It should also be noted that the cost to change

the current inspection method, which has been used for around 15-20 years and has already produced massive amounts of historical condition rating records, is expensive. Any change to the inspection method will also create data incompatibility issues; and (iii) a number of safety risks are associated with bridge inspectors (Lim et al. 2011). A bridge inspection is performed directly on the bridge, thus conducting visual inspections of a bridge deck contains risks with passing traffic. In practice, some bridge elements also have accessibility issues. Therefore the inspector may need to be stationary on a temporary platform on an inspection vehicle in order to accurately judge the bridge element conditions; (iv) bridge inspections require highly experienced and trained personnel, which is now a challenging issue for most bridge authorities as there is a shortage of the required level of inspectors (Zhu et al. 2010). Moreover, insufficient training, vision problems, accessibility and location can cause inconsistencies in visual inspections (Sterritt 2009). These limitations can cause further unreliable predictions of long-term bridge performance on the basis of the deterioration model in a BMS.

In order to minimise the aforementioned limitations, a feasibility study has been performed to enhance the current visual inspection method using optical image processing techniques. However, the method developed is not fully capable of addressing the challenges in automatic crack detection. These challenges include variable lighting conditions, random camera/view angle, and random resolution of bridge images. This paper thus proposes a new bridge inspection approach employing wavelet-based image features along with SVMs for automatic detection of cracks in bridge images. A two-stage approach is followed, whereby in the first stage, upon initially analysing the characteristics of the pixel values in 'R', 'G' and 'B' channels, the image is identified as either a 'complex' or a 'simple' image. If the image is identified as a 'complex image' then a pre-processing step is executed otherwise the image is directly processed for feature extraction. Using a non-overlapping sliding window, texture analysis–based features are extracted from the image region beneath the sliding window. Later in the second stage, the extracted features are passed on to a SVM classifier to decide whether the region beneath the sliding window contains a crack or not. The outcome of the proposed method indicates that an overall accuracy of 92% is obtained even when undertaking experiments with noisy and complex bridge images.

2 RELATED WORKS ON CRACK DETECTION

Outlined herein are some of the research efforts made on automated crack detection of bridge images using image processing and pattern recognition techniques.

Ehrig et al. (2011) introduced three different crack detection algorithms namely template matching, sheet filtering based on hessian eigenvalues, and percolation based on the phenomenon of liquid permeation. Their study focused on determining the suitability of each for crack detection. Subsequently, the percolation algorithm was modified using employing a sheet filter approach for application to three-dimensional images. It should be noted that the template matching technique was used to detect certain patterns. The latter was based on the physical model of liquid permeation, with each pixel considered to be either a crack or otherwise. As a result, the modified percolation algorithm, called 'Hessian-driven percolation', verified its effectiveness in crack detection. It was found, however, that the Hessian-driven percolation was not suitable for thin cracks.

Abdel-Qader et al. (2003) compared edge-detection algorithms in the context of bridge crack detection. Collections of 50 concrete bridge images were used. Four techniques were also employed for comparative analysis: fast Haar transform (FHT), fast Fourier transform (FFT), Sobel edge detection, and Canny edge detection. The output images were judged as containing cracks or no cracks based on a threshold, which was determined by the average value of the intensity of all pixels in the images. The conclusion drawn was that the FHT performed significantly better than the other algorithms.

Jahanshahi and Masri (2011) presented a feasibility study on a novel crack detection methodology for condition assessment of concrete structures. Such an assessment was performed in three steps including: (a) image acquisition; (b) image processing (segmentation and feature extraction); and (c) pattern recognition (classification). After the target images were collected, morphological operation and Otsu's thresholding method were adopted to the segmentation process. The purpose of the segmentation process was to reduce unnecessary data in the original image. The appropriate structure element size (in pixel) was also determined for a morphological operation based on camera focal length, the distance from the object to the camera, camera sensor resolution and size, as well as crack thickness. Following the process of image processing, five features were selected to feature extraction based on the Linear Discriminant Analysis (LDA). For comparative

analysis in the classification process, Neural Network, Support Vector Machine and Nearest Neighbour were used. Analysis results suggested that, Neural Network was better than the other techniques.

Mohajeri and Manning (1991) established a recognition system for segmented concrete crack images. The system uses directional filters to identify cracks in concrete. The crack can be identified to be longitudinal if there is a high concentration of object pixels in a narrow interval of x (transverse) coordinates, and to be transverse if there is a large number of object pixels in a narrow interval of y (longitudinal) coordinates. However, this system has been found to have difficulties in collecting accurate segmented crack images.

Tong et al. (2011) developed a new method of crack image processing for concrete bridges in order to collect high quality images. Their work recognised that images introduce noise such as irregular illumination, presence of moisture on concrete surfaces and shading. These problems induce unreliable outcomes of concrete crack detection. To minimise these problems, their method involves a preprocessing phase and then separates crack pixels from the background of the image through manipulation of grey level correction. However, this method is highly dependent on light conditions and it requires changing the average grey level of images.

A review of literature indicates that the abovementioned methods do not consider the images with difficult visual and are unable to process the bridge images with variable lighting conditions, random camera/view angle, and random resolution. Applying automatic visual bridge inspection method usually encounters difficulties in terms of the qualities of bridge images. How to automatically process the low quality bridge images and achieve reliable crack detection outcomes are vital in bridge condition assessment.

3. IMAGE ACQUISTION AND DATASET DETAILS

In the present study, the photography equipment used for capturing bridge images comprises a Canon 5D Mark II camera with Canon 24–70 mm and 70–200 mm lenses. The captured colour images have a resolution of 5616 × 3744 (21 megapixels). With these settings, the proposed system is capable of taking images of a 561.6 × 374.4 mm area and detecting Condition State 1 (a crack width of less than 0.1 mm). A total of 50 images of different concrete bridge elements are collected. The images are taken with different backgrounds and on different surfaces and light exposure conditions. In total, 1,369 "window" regions of type 'crack' and 'non-crack' are obtained from the collected 50 images.

4. THE PROPOSED AUTOMATIC CRACK DETECTION SYSTEM

In order to analyse the bridge image locally, a sliding window strategy is deployed. For better computational efficiency, a non-overlapping 30 × 40 pixel window is glided over the entire image and the region beneath each window called 'window regions' is classified into a 'crack' or 'non-crack' region by a SVM classifier (refer to Section 4.3). The size of the sliding window is set after empirically experimenting on the images. It is noted that the cracks in the images are at most 25 pixels in width. As such, a 'crack' region is assumed to contain a crack with the background component, whereas a 'non-crack' region should cover the background element only.

During the initial research, it was noted that the features (refer to Section 4.2) were capable of performing well when the images consisted of a near consistent background with a high contrast between the foreground and the background, which can be termed as a 'normal' image. The feature was not performing well with 'complex' images, which had sudden changes in intensities in both the foreground and background, or when the images are dull in nature (where the background gets fused with the foreground). It is noted that for 'normal' images, the values of the 'R', 'G' and 'B' channels for a pixel are very similar to each other (low standard deviation for all three values) and the range of these values are quite wide. However for 'complex' images, the values of the 'R', 'G' and 'B' channels for a pixel are quite different from each other (high standard deviation for all three values) with relatively small range. Using this heuristic information, all input images can broadly be clustered into two groups – 'complex' and 'normal'. Examples of 'complex' and 'normal' bridge images are shown in Figure 1.

After an image is categorised as 'complex', further processing is required so that the crack mark becomes prominent with respect to its surroundings. After undergoing a series of colour space conversions and filtering of values in various colour space channels, an equivalent grey scale image of the complex image was obtained. Furthermore, if the grey scale equivalent image of the 'complex' images can be processed by a contrast stretching algorithm, then the same features become effective. To achieve this, a two-stage approach is taken to deal with the process. The first stage is to decide whether an image is of the type 'complex' or 'normal'. For a

'complex' image, the pre-processing method (refer to Section 4.1) is undertaken for the whole image and then the processed results are forwarded to the feature extraction phase. For a 'normal' image, the pre-processing method is not required and instead the image can be directly used to extract features. It should be noted that the proposed approach, in its present form, is unable to procure a large number of bridge images. In view of this, a five-fold cross-validation scheme is implemented instead of dividing the entire corpus into training and test subsets.

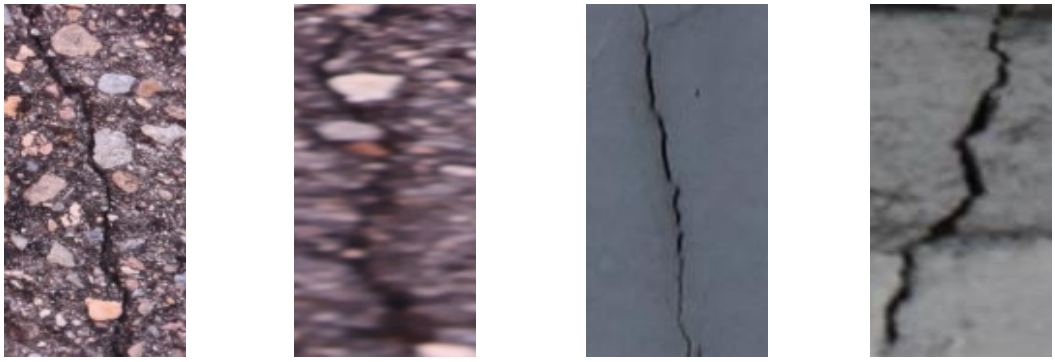

(a) Two 'complex' images (b) Two 'normal' or 'standard' images

Figure 1. 'Complex' and 'normal' bridge images.

The features extracted from all 'crack' and 'non-crack' windows are combined and all the feature vectors are subsequently divided into five sets: four for training and the remaining one for testing. The process is repeated four more times so that each of the remaining four sets in the last training set can be employed for testing. It is noted that if the five-fold cross-validation scheme involving feature vectors from both 'complex' and 'normal' images are simultaneously implemented, then the accuracy can be diminished. Further investigation results indicate that mostly feature vectors from 'complex' images were incorrectly classified. Even by tuning the values of the SVM parameters, the situation did not change. Only after removing all feature vectors that belonged to the 'complex' image category, did the accuracy improve. However, upon implementing a five-fold cross-validation scheme, the feature vectors obtained exclusively from the 'complex' images, exhibit similar accuracy to those obtained on 'normal' images. It is worth mentioning here that the optimised parameters for feature vectors from two different image types are quite different.

4.1 Pre-processing method

Only those images that have been identified as a 'complex' type image in the first stage will be executed through pre-processing. Figure 2 is example for applying pre-processing method. The images are originally in RGB format, and are then transformed to a HSV colour space. The reason behind this is that in HSV space the image intensity can be separated from the colour information. Also such a transformation for 'complex' type images can ensure robustness against lighting changes, and shadows. In the HSV colour space, 'Hue' defines the colour component and ranges between 0-1.0, and 'Saturation' describes how white the colour is, whereas the 'Value' defines the lightness component in a pixel (0 means white and 1 means complete black). During the initial research, it was noticed that highlighting the crack in an image could be achieved by analysing the Hue and Saturation channel values, which can subsequently be manipulated to the desired values. If in a pixel the Hue value is >=0.9 and the corresponding Saturation value is <= 0.2, then it can be assumed that Hue = 0.6, Saturation= 1.0 and Value (intensity/brightness) = 0.1; otherwise the saturation is set to 0.2 and the remainder of the two channel values were kept intact. With the former case, ensuring that the crack pixels present a proper blue colour with dark shade (see Figure 2(b), in the Hue axis 0.6 resembles blue and Saturation 1 ensures that the pixel can be visually perceived as the true blue, the low intensity value ensures darkness with respect to the surroundings). With the latter case, the remaining pixels must be ensured to have more of a grey-like shade by applying a low saturation value. From the final output image presented in Figure 2(f), it is clearly evident that the pre-processing steps can easily convert a 'complex' image type as shown in Figure 2(a) to appear the same as a 'normal' image. Upon comparison of Figure 2(b) and Figure 2(f), it is evident that they appear visually similar.

The pre-processing steps can be outlined as follows:

(a) Transform RGB to HSV colour space;
(b) Check the range of Hue and Saturation values in a pixel and set the values of all H, S, V channels accordingly;
(c) Conversion to RGB;
(d) Convert the RGB to Grey scale;
(e) Perform contrast stretching on the grey scale image;
(f) Undertake final filtering on grey scale values (fix all grey scale values above a threshold to one particular high grey scale value) to obtain the desired output image.

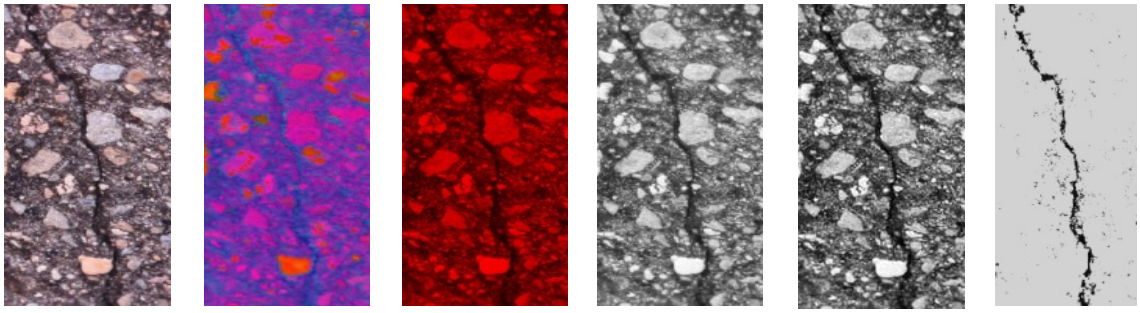

(a) (b) (c) (d) (e) (f)

Figure 2. (a) Extreme left an original input image; (b)-(e) same image in various intermediate stages; (f) extreme right corresponding to the final output image after pre-processing.

4.2 Feature extraction method

A comparative analysis between different texture analysis-based methods is conducted for the purpose of crack detection. All the different features are extracted from the sliding window that glides over the whole image. Three different texture-analysis based features, such as Zernike moment features, Gabor filter features and Daubchies Wavelet features, are investigated. Consequently, the performance of wavelet features is proven to outperform the other two features during experimentation. Details of this comparative analysis are outlined below.

Zernike moments Zernike moment features are rotation invariant in nature. Two dimensional Zernike moments can be computed using the formula:

$$A_{mn} = \frac{m+1}{\pi} \int_x \int_y f(x,y)[V_{mn}(x,y)]^* \, dx\, dy \qquad (1)$$

where, $x^2 + y^2 \le 1$ and $m - |n| = even, |n| \le m$

In Eq. (1), m = 0, 1, 2… ∞ defines the order and f(x, y) is the function being described and * denotes the complex conjugate. *n* is an integer implying the angular dependence. For a discrete image pixel P(x, y), the integrals are changed to summation, and Eq. (1) is transformed to the following:

$$A_{mn} = \frac{m+1}{\pi} \sum_x \sum_y P(x,y)[V_{mn}(x,y)]^* \qquad (2)$$

where, $x^2 + y^2 \le 1$

For the proposed study, the idea is to map the image of the size-normalised image patches (the area beneath the sliding window) to the unit disc using polar coordinates, where the centre of the image is the origin of the unit disc. Those pixels falling outside the unit disc are not used in the proposed computation. More details of the Zernike moment features can be found in (Khotanzad and Hong 1990).

Gabor filter Gabor filters are capable of representing signals in both a frequency and a time domain. A two-dimensional Gabor filter in a spatial and frequency domain can be defined by the following formula:

$$G(x, y, \lambda, \theta, \psi, \sigma, \gamma) = \exp\{(x'^2 + \gamma^2 y'^2)/2\sigma^2\} \cos(2\pi x'/\lambda + \psi) \qquad (3)$$

where, $x' = x\cos\theta + y\sin\theta$; $y' = -x\sin\theta + y\cos\theta$

In Eq. (3), the wavelength of the cosine factor is represented by λ, θ represents the orientation of the normal to the parallel stripes of a Gabor function, ψ denotes the phase offset, the sigma of the Gaussian envelope is represented by σ and γ represents the spatial aspect ratio that specifies the ellipticity of the support of the Gabor function. A combination of different values of these parameters has been tested, and the optimised results are achieved when the spatial frequency is set to 21/2, and δ set to 2*π.

Wavelet features wavelet transform is a useful technique in analysing non-stationary signal in time-frequency domain. Initially, the Haar-wavelet transform and Daubechies wavelet transform features were investigated, with Daubechies wavelet providing better test outcomes. Daubechies wavelets are a family of orthogonal wavelets defining a discrete wavelet transform. This consists of four scaling function coefficients and four wavelet function coef-

ficients. The former coefficients presented below are used by the proposed test:

$$\frac{1+\sqrt{3}}{4\sqrt{2}}, \frac{3+\sqrt{3}}{4\sqrt{2}}, \frac{3-\sqrt{3}}{4\sqrt{2}}, \frac{1-\sqrt{3}}{4\sqrt{2}}$$

After connected-component labelling is done on the binary image, the bounding box of all character-components is obtained. The input grey images within the bounding box are copied. The features are extracted after size normalizing each such grey scale image of the sliding windows to 32 × 32 dimensions. Details of the feature can be found in (Daubechies 1990).

4.3 Support vector machine (SVM) classifier

SVMs are employed as the classifier in this study. SVMs are defined for two-class problems and search for an optimal hyper plane, which maximizes the distance and the margin between the nearest examples of both classes, namely vectors (SVs). Given a training database of M data: {Xm|m=1,..., M}, the linear SVM classifier is then defined as:

$$f(x)=\sum_j \alpha_j y_j x_j \cdot x + b \tag{4}$$

where, $\{x_j\}$ are the set of SVs and the parameters α_j and *b* are determined by solving a quadratic problem (Burges 1998). The linear SVM can be extended to various non-linear variants, and details can be found in (Burges 1998; Vapnik 1995). According to the test results, it is noted that the Gaussian kernel SVM outperforms the other non-linear SVM kernels. Hence, the Gaussian kernel, presented in the following form, is employed to report the recognition results.

$$[k(x,y)=\exp(-\frac{\|x-y\|^2}{2\sigma^2})] \tag{5}$$

The best kernel parameters are selected by means of a series of validation experiments. The best optimized results are obtained when $(1/2\sigma^2)$ is set to values such as 80.00 (while dealing with 'normal' images) and 9.00 (while dealing with 'complex' images) with the penalty multiplier value set to 1.

5. RESULTS AND DISCUSSION

Further analyses have been conducted according to the results obtained to provide more insights to the proposed method. When five-fold cross validation is implemented separately on feature vectors from 'complex' and 'normal' images, higher accuracy can be achieved as compared to when implementing five-fold cross validation on feature vectors for both image types. Here, the accuracy employing only wavelet features is reported, which is depicted in Table 1. As the table shows, 81% of accuracy is obtained when feature vectors are considered from both 'complex' and 'normal' images. Similarly while considering feature vectors from only 'normal' images, 93% of accuracy can be achieved (873 correctly classified considering 936 samples from 'normal' images during a five-fold cross validation) whereas while considering feature vectors from only 'complex' images (388 correctly classified considering 433 samples during cross validation), an accuracy of 90% can be obtained. Thus the average accuracy achieved by the proposed approach becomes 92%. The distribution of the confidence score during the classification process (cumulatively for 'complex' and 'normal' images) is described in Section 5.1 confirming the overall accuracy of the approach. In Section 5.2, the performance of the proposed approach is inspected by training it using feature vectors exclusively obtained out of one particular image type ('complex'/'normal') and testing it on the other image type. Sections 5.3 and 5.4 are dedicated to comparative analysis of three different features and error analysis, respectively.

Table 1. Effect of training image types on accuracy.

Training set type	Accuracy
Complex image and normal image	81%
Normal image	93%
Complex image	90%
Average	92%

5.1 Distribution of confidence score on top-choice classification

The confidence score implies the probability estimation of the recognized class. It is noticed that a large section of the correct classifications have a confidence score in the range of 0.8-1.0. This is depicted in Figure 3. A large percentage of correct classification with high confidence score indicates that our wavelet-based features are robust in nature.

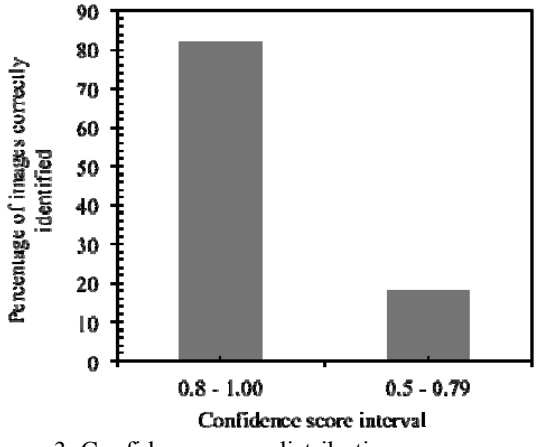

Figure 3. Confidence score distribution.

5.2 Effect on performance due to complex (normal) images in training (test) set

As mentioned in earlier experiments, this study involves two different types of images: 'complex' and 'normal'. It is interesting to investigate when only training the classifier with feature vectors of "crack" and "non-crack" image regions obtained from all 'complex' ('normal') regions and testing them with these regions obtained from all 'normal' ('complex') images. According to the results of the earlier experiments, the highest accuracy is obtained while using wavelet features. These results are presented in Table 2 and it can be concluded that 'normal images' are much better for use in the training set and provide a more generalised learning model.

Table 2. Effect of training image types on accuracy.

Training set type	Test set type	Accuracy
Complex image	Normal image	79% (739 out of 936)
Normal image	Complex image	87% (377 out of 433)

5.3 Comparison with other texture analysis based features

Table 3 compares three different feature extraction methods. Note that the accuracy is reported while dealing with all feature vectors simultaneously irrespective of the image types (complex/normal). The highest accuracy is obtained with wavelet features, outperforming the other two feature extraction methods.

Table 3. Comparison between three different features.

Feature used	Accuracy
Zernike moments	61%
Gabor filter	74%
Wavelet	87%

5.4 Error analysis

Upon analysing the errors, it is noted that most of the time 'window regions' with a blurred appearance are misclassified to the wrong class. This happened to 'window regions' obtained from both 'complex' and 'normal' image types where the foreground element is not prominent compared to the background element in the images and that they tend to fuse with each other. Nevertheless it is worth mentioning here that in such images our contrast stretching algorithm does not perform very well, which is one of the reasons for not recognising the cracks. An example of such an image is shown in Figure 4. It should be noted that the region marked within the rectangular area highlights a crack mark, which is almost invisible there, however the crack mark is more visible in regions above the rectangular area.

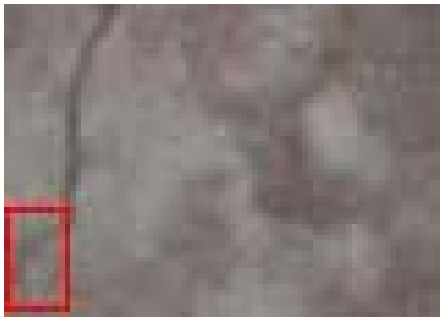

Figure 4. An invisible crack mark within the rectangular region.

6. CONCLUSION

The problems of automatic bridge crack detection have been investigated employing real-world bridge images. The proposed method has demonstrated its capabilities to deal with all the images collected from bridge inspections including both 'normal' and 'complex' images. The pre-processing procedure of the proposed method was employed to handle the 'complex' images and three different features (Zernike moments, Gabor filter and Wavelet) were used to automatic detect the images with or without cracks. The comparison results indicated that the Wavelet-feature method could provide most accurate results by achieving an average accuracy of 92% even when dealing with very complex bridge image types. Such a high accuracy achieved in this phase of the study will enhance the accuracy of the crack width measurement and in turn improve the reliability of the automated bridge inspection system.

Future work includes autonomous image data acquisition using devices such as robots or unmanned aerial vehicles (UAVs). Obtaining an image at a specific position in high precision is not a trivial task, when using an autonomous device. Various sensors, such as optical, acoustic and magnetic sensors, may aid in this task. Multiple sensors, based on individual specialties, are commonly used in order to complement limitations imposed by certain sensors and thus enriching the perception of single sensors. It should be noted however that, it is challenging to integrate the heterogeneous types of sensory information and produce useful results. A pilot study of the likelihood-based data fusion system has been implemented for robot positioning (Jo and Tsunoda 2013; Jo et al. 2013). This system integrates a light detection and range (Lidar), a vision sensor (a webcam) and an inertial measurement unit (IMU). The implementation results have already shown promising results (Jo and Tsunoda 2013).

7. ACKNOWLEDGEMENT

The resources used for the present study were provided by the Department of Engineering Services, Gold Coast City Council (GCCC), Australia, which enabled the preliminary study to be successfully completed. The authors would like to thank Mr. Randall Scott, Ms. Yvonne Ulas, and Mr Bill Zhang from the GCCC for their assistance with the data collection process.

8. REFERENCES

Phares, B.M., Washer, G.A., Rolander, D.D., Graybeal, B.A. and Moore, M. "Routine highway bridge inspection condition documentation accuracy and reliability," *J. of Bridge Engineering*, 9 (4), 2004, 403–413.

Moore, M., Phares, B., Graybeal, B., Rolander, D. and Washer, G. "Reliability of visual inspection for highway bridges," *Volume I: Final Report and, Volume II: Appendices, U.S. Department of Transportation*, Washington, D.C, FHWARD-01-020 (021), 2001.

Chase, S. and Edwards, M. "Developing a telerobotic platform for bridge inspection," University of Virginia, USA, 2011.

Sanford, K.L., Herabat, P. and Mcneil, S. "Bridge management and inspection data: leveraging the data and identifying the gaps," *Transportation Research Board 8th International Bridge Management Conference*, Denver, Colorado, 1999.

Lim, R.S., La, H.M., Shan, Z. and Sheng, W. "Developing a crack inspection robot for bridge maintenance," *IEEE Conference Publication*, 2011, pp. 6288-6293.

Zhu, Z., German, S. and Brilakis, I. "Detection of large-scale concrete columns for automated bridge inspection," *Journal of Automation in Construction*, 19 (8), 2010, 1047-1055.

Sterritt, G. "Review of Bridge Inspection Competence and Training. Project Report," www.bridgeforum.org/bof/projects/bict/Bridge%20Inspector%20Training%20and%20Competence%20Phase%201%20Report%20Final.pdf (2009, accessed 23 January2012).

Ehrig, K., Goebbels, J., Meinel, D., Paetsch, O., Prohaska, S. and Zobel, V. "Comparison of crack detection methods for analysing damage processes in concrete with computed tomography," *Proceedings of International Symposium on Digital Industrial Radiology and Computed Tomography*, Berlin, Germany, P2, 2011.

Abdel-Qader, I., Abudayyeh, O. and Kelly, M.E. "Analysis of edge-detection techniques for crack identification in bridges," *Journal of Computing in Civil Engineering*, 17(4), 2003, 255-263.

Jahanshahi, M.R. and Masri, S.F. "A novel crack detection approach for condition assessment of structures," *ASCE International Workshop on Computing in Civil Engineering*, Miami, Florida, 2011, pp. 388–395.

Mohajeri, M.H. and Manning, P.J. "ARIA: An operating system of pavement distress diagnosis by image processing," *Transportation Research Record*, 1991, No 1311, 120–130.

Tong, X., Guo, J., Ling, Y. and Yin, Z. "A new image-based method for concrete bridge bottom crack detection," *Image Analysis and Signal Processing*, Hubei, China, 2011, pp. 568–571.

Khotanzad, A. and Hong, Y.H. "Invariant image recognition by Zernike moments," *IEEE Transactions on PAMI*, 12(5), 1990, 489–497.

Daubechies, I. "The wavelet transform, time-frequency localization and signal analysis," *IEEE Transactions on Information Theory*, 36(5), 1990, 961-1005.

Burges, C. "A tutorial on support vector machines for pattern recognition," *Data Mining and Knowledge Discover 2*, 1998, pp. 121-167.

Vapnik, V. "The nature of statistical learning theory," Monograph 2nd ed. 2000, XIX, 1995, 314p.

Jo, J.H. and Tsunoda, Y. "A data fusion model based on ROI and Likelihood for the integration of multiple sensor data," Accepted and will appear in the Proceedings of the 2nd International Conference on Robot Intelligence Technology and Applications 2013, Springer, Germany.

Jo, J.H., Tsunoda, Y., Sullivan, T., Lennon, M. and Jo, T. "BINS: Blackboard-based Intelligent Navigation System for multiple sensory data integration," The 17th International Conference on Image Processing, Computer Vision, & Pattern Recognition, Nevada, 2013, USA.